JOURNAL OF THE AMERICAN CHEMICAL SOCIETY

Article

Pushing the Limits on Metal–Organic Frameworks as a Catalyst Support: NU-1000 Supported Tungsten Catalysts for o-xylene Isomerization and Disproportionation

Sol Ahn, Scott L Nauert, Cassandra T. Buru, Martino Rimoldi, Hyeju Choi, Neil M. Schweitzer, Joseph T. Hupp, Omar K. Farha, and Justin M Notestein

J. Am. Chem. Soc., **Just Accepted Manuscript** • DOI: 10.1021/jacs.8b04059 • Publication Date (Web): 17 Jun 2018

Just Accepted

ACS Publications

is published by the American Chemical Society. 1155 Sixteenth Street N.W., Washington, DC 20036

Pushing the Limits on Metal–Organic Frameworks as a Catalyst Support: NU-1000 Supported Tungsten Catalysts for *o*-xylene Isomerization and Disproportionation

Sol Ahn,[†] Scott L. Nauert,[†] Cassandra T. Buru,[‡] Martino Rimoldi,[‡], Hyeju Choi,[‡] Neil M. Schweitzer,[†] Joseph T. Hupp,[‡] Omar K. Farha,[*†‡§] and Justin M. Notestein[*†]

[†]Department of Chemical and Biological Engineering, and [‡]Department of Chemistry, Northwestern University, 2145 Sheridan Road, Evanston, Illinois 60208, United States

[§]Department of Chemistry, Faculty of Science, King Abdulaziz University, Jeddah 21589, Saudi Arabia

■ ABSTRACT

Acid-catalyzed skeletal C-C bond isomerizations are important benchmark reactions for the petrochemical industries. Among those, *o*-xylene isomerization/disproportionation is a probe reaction for strong Brønsted acid catalysis, and it is also sensitive to the local acid site density and pore topology. Here, we report on the use of phosphotungstic acid (PTA) encapsulated within NU-1000, a Zr-based metal–organic framework (MOF), as a catalyst for *o*-xylene isomerization at 523 K. Extended X-ray absorption fine structure (EXAFS), ^{31}P NMR, N_2 physisorption, and XRD show that the catalyst is structurally stable with time-on-stream, and that WO_x clusters are necessary for detectable rates, consistent with conventional catalysts for the reaction. PTA and framework stability under these aggressive conditions requires maximal loading of PTA within the NU-1000 framework; materials with lower PTA loading lost structural integrity under the reaction conditions. Initial reaction rates over the NU-1000-supported catalyst were comparable to a control WO_x-ZrO_2, but the NU-1000 composite material was unusually active toward the transmethylation pathway that requires two adjacent active sites in a confined pore, as created when PTA is confined in NU-1000. This work shows the promise of metal–organic framework topologies in giving access to unique reactivity, even for aggressive reactions such as hydrocarbon isomerization.

KEYWORDS: *metal–organic framework, solid acid, polyoxometalate, phosphotungstic acid, heterogeneous catalysis, supported catalyst, o-xylene, isomerization, disproportionation*

■ INTRODUCTION

Isomerization and disproportionation reactions of hydrocarbons such as hexane and xylene are crucial reactions in the production of fuels and basic petrochemicals, and these reactions have also long been model reactions that provide structural information on solid acid catalysts.[1-3] Tungstated zirconia (WO_x-ZrO_2) is one example of a material capable of carrying out a wide range of solid acid catalysis such as alkane isomerization,[4-5] alcohol dehydration[6] and etherification,[7] and *o*-xylene isomerization.[8-10] WO_x-ZrO_2 is typically synthesized by impregnation on amorphous supports and subsequent calcination. These materials have very strong structure sensitivity,[11] in which the structure of the active material strongly influences the rate. As such, the use of conventional syntheses that cause heterogeneity of active sites can complicate the understanding of the material's overall reactivity. Phosphotungstic acid (PTA, $H_3PW_{12}O_{40}$) is a Keggin polyoxometalate (POM) cluster that can provide the tungsten oxide active sites for the aforementioned model reactions owing to its activity for acid catalysis. For instance, pure PTA has been reported for depolymerization of polytetrahydrofuran[12] and alkylation of toluene.[13] Researchers have extensively studied PTA as heterogeneous acid catalysts on various supports. Kukovecz et al. reported sol-gel incorporation of PTA on silica for alkene isomerization,[14] Devassy et al. impregnated PTA on zirconia for phenol alkylation,[15] and Macht et al. deposited PTA on SiO_2 via incipient wetness impregnation for alcohol dehydration.[16]

Separately, many researchers have been studying metal–organic frameworks (MOFs) as catalyst supports potentially capable of creating uniform active sites placed in controlled pore environments.[17-20] It is generally hypothesized that catalysts with more uniform and isolated active sites will lead to better understanding of the catalytic surface phenomena.[21-22] In addition, MOFs have various applications in many fields such as gas storage and separation,[23-27] drug delivery,[28] or sensors.[29-30] In particular, the zirconium-based MOF, NU-1000, possesses outstanding chemical and hydrothermal stability relative to many MOFs.[31-32] Further, the hexa-zirconium (Zr_6) nodes are only 8-connected via tetracarboxylate (1,3,6,8-tetrakis(p-benzoate)pyrene, $(TBAPy)^{4-}$) linkers, providing four additional grafting sites on each node in the form of four terminal and four bridging hydroxyl groups. The size of the tetracarboxylate linkers places each Zr_6 cluster at least 1.0 nm from one another, ensuring site isolation for small grafted species such as single metal ions.[33-34] Finally, three distinct pore openings are created with csq-net topology. Hexagonal and triangular pores of 3.1 and 1.2 nm,

respectively, are aligned along the a-axis, while 1.0 nm rhomboid pores are aligned along the c-axis (Figure 1).[35]

Recently, Zhang et al. encapsulated PTA in MIL-101, a Cr-based MOF, for sugar dehydration.[36] Also, Wang et al. synthesized WO_x-ZrO_2 using UiO-66 as a precursor for acetalization of benzaldehyde.[37] These studies among others[38-43] have furthered the development of MOF-based Brønsted-acidic catalysts, but in some cases, MOFs are unstable under the reaction conditions. In this study, we encapsulate a high weight-loading of PTA within NU-1000 and show that the POM and MOF structures remain intact following the representative strong acid-catalyzed reaction of *o*-xylene isomerization/transmethylation. The structures and reactivities of NU-1000-supported PTA catalysts are compared to a reference WO_x-ZrO_2 and to a WO_x-loaded NU-1000 synthesized by an alternate route. To the best of our knowledge, this work provides the first example of an acid-catalyzed, hydrocarbon skeletal isomerization reaction – a class of important benchmark strong Brønsted acid-catalyzed reactions for the petrochemicals industries – occurring within a MOF.

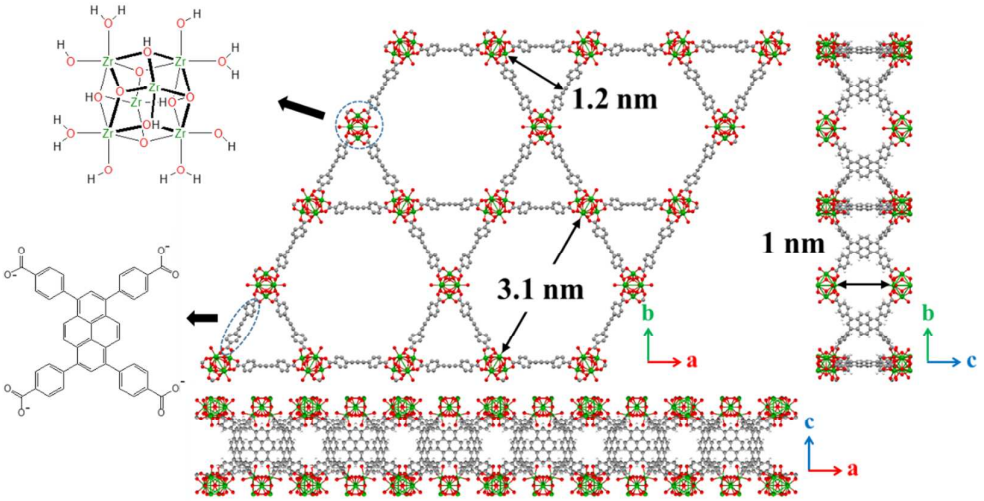

Figure 1. Crystal structure of NU-1000. The structures of Zr_6 node (top left) and organic linker (bottom left) are given. Dark green=Zr, red=O, gray=C, white=H

■ RESULTS AND DISCUSSION

Synthesis and Characterization.

Table 1 summarizes the bulk properties of the W-loaded catalysts synthesized in this study. The reference WO_x-ZrO_2 possesses 16.5 wt% W, corresponding to 1.6 W/nm^2, or 22% of a monolayer (0.22 W/Zr_{surf}), when considering the N_2 physisorption surface area and Zr atom surface density of the original support. W-SIM (Solution phase grafting in MOFs) is synthesized by a self-limiting method that gives a similar W loading by mass, but a much lower surface density based on total N_2 physisorption surface area, due to the high total surface area of the MOF. However, surface density may be more useful if normalized to surface zirconium atoms, since W will not be grafted directly on the organic linkers. Assuming that all the Zr atoms in the nodes are accessible, W-SIM reaches 0.41 W/Zr_{surf} or 2.5 W per Zr_6 node. This loading is typical of deposition of mononuclear precursors by grafting or atomic layer deposition (ALD) within NU-1000, which typically does not exceed 4 metals per Zr_6 node when the MOF is intact.[21-22, 44-47] In W-SIM, ^{1}H NMR confirmed the complete removal of the precursor ligands (*tert*-butylimido and dimethylamino) and thus the conversion of W-N and W=N into a supported WO_x. Finally, two different loadings of PW_{12}@NU-1000 are synthesized by exposure of NU-1000 to aqueous PTA solutions. To synthesize 0.5 PW_{12}@NU-1000, NU-1000 is exposed to 0.5 equivalents of PTA to one Zr_6 node resulting in loadings of 30.6 wt% W, 0.4 W/nm^2 total N_2 physisorption surface area, and 0.9 W per surface Zr. To obtain higher POM loading, 0.9 PW_{12}@NU-1000 was synthesized with two equivalents of PTA per Zr_6, following a previously published procedure.[48] Our team previously demonstrated the uniform distribution of PTA within the NU-1000 in the case of 0.9 PW_{12}@NU-1000 using SEM-EDX;[48] we confirm here a similarly uniform distribution of PTA within 0.5 PW_{12}@NU-1000 as well (Figure S1). With exposure to excess PTA, the material contains 44.9 wt% W, corresponding to 0.5 W/nm^2, or 1.7 W/Zr_{surf}. This is equivalent to 10.3 W per Zr_6 node or 0.86 POM per Zr_6 node; approximately 1 POM per node appears to be the maximum value. After loading the W-containing species, W-SIM and the two PW_{12}@NU-1000 samples have lower surface areas than the original NU-1000 based on gravimetric surface area, as expected, and these composites still possess the characteristic mesopores (step around P/P_o=0.2-0.25 in Figure 2a and pore widths in Figure 2b) as well as micropores of NU-1000. Additionally, diffuse reflectance infrared Fourier transform (DRIFT) spectra (Figure S2) show a decrease in the O-H stretch (3670 cm^{-1}) from the non-H bonded

hydroxyl and aqua ligands for both W-SIM and 0.9 PW_{12}@NU-1000 relative to the starting material, consistent with anchoring/encapsulation of WO_x clusters via the hydroxyl ligands of NU-1000.

Table 1. Summary of catalysts.[a]

Catalyst	W loading [wt% W]	W loading [W/Zr_6 node]	BET Surface area [$m^2/g_{catalyst}$]	Volumetric Surface area [$m^2/cm^3_{NU-1000}$]	Surface density [W/nm^2]	Surface density [W/Zr_{surf}]
ZrO_2	n/a	n/a	270	n/a	n/a	n/a
WO_x-ZrO_2	16.5	n/a	125[b]	n/a	1.59	0.22[b]
NU-1000	n/a	n/a	2160	1050	n/a	n/a
W-SIM	17.0	2.5	930[c]	560	0.20	0.41[c]
0.5 PW_{12}@NU-1000	30.6	5.4	1150[c]	840	0.37	0.90[c]
0.9 PW_{12}@NU-1000	44.9	10.3	740[c]	700	0.54	1.72[c]

[a] Values were reproducible to within ± 3.5 % from three different catalyst synthesis batches
[b] Calculated based on surface Zr density of zirconia,[49-50] 7.34 Zr/nm^2
[c] Assuming every Zr of NU-1000 node is exposed on the surface

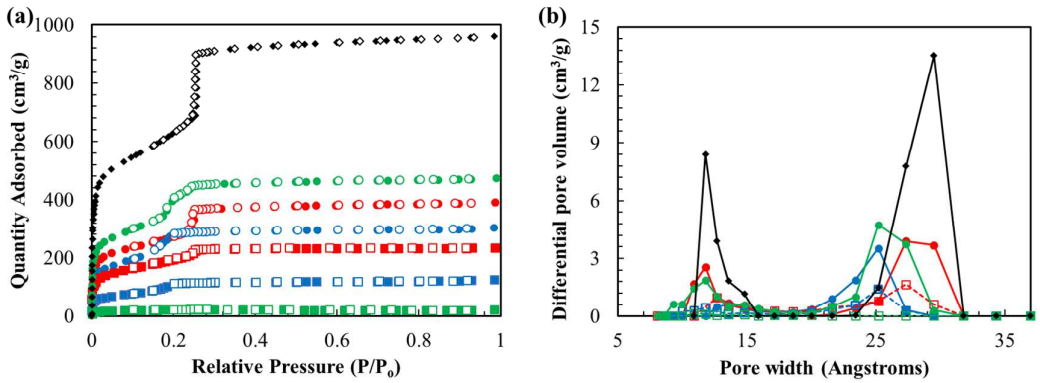

Figure 2. (a) N_2 physisorption adsorption/desorption isotherms and (b) DFT (carbon slit pore N_2 77 K kernel) pore size distributions of NU-1000 (black), W-SIM (red), 0.5 PW_{12}@NU-1000 (green), and 0.9 PW_{12}@NU-1000 (blue). Circles: as synthesized, squares: after catalysis.

Considering the W loadings and surface densities alone, the two PW_{12}@NU-1000 catalysts and the control WO_x-ZrO_2 are expected to contain some active WO_x clusters, while the W-SIM may possess highly dispersed W atoms that would not be catalytically active. In addition, the relatively low diffuse reflectance UV-vis (DRUV-vis) edge energy of WO_x-ZrO_2 of 2.95 eV (Figure S3) is consistent with the presence of WO_x clusters.[8] DRUV-vis is unfortunately not diagnostic for NU-1000 supported catalysts due to the strongly-absorbing organic linkers

that overlap the WOx edge.

PXRD patterns (Figure 3a) show that the long-range order of the MOF framework in W-SIM and 0.9 PW_{12}@NU-1000 are maintained upon W deposition and after *o*-xylene isomerization reaction conditions. Peak broadening observed in the case of W-SIM after catalysis might indicate partial loss of structural integrity. For the as-synthesized PW_{12}@NU-1000 catalysts, these patterns have been previously assigned to the presence of POM clusters located in the small triangular channels of NU-1000.[48]

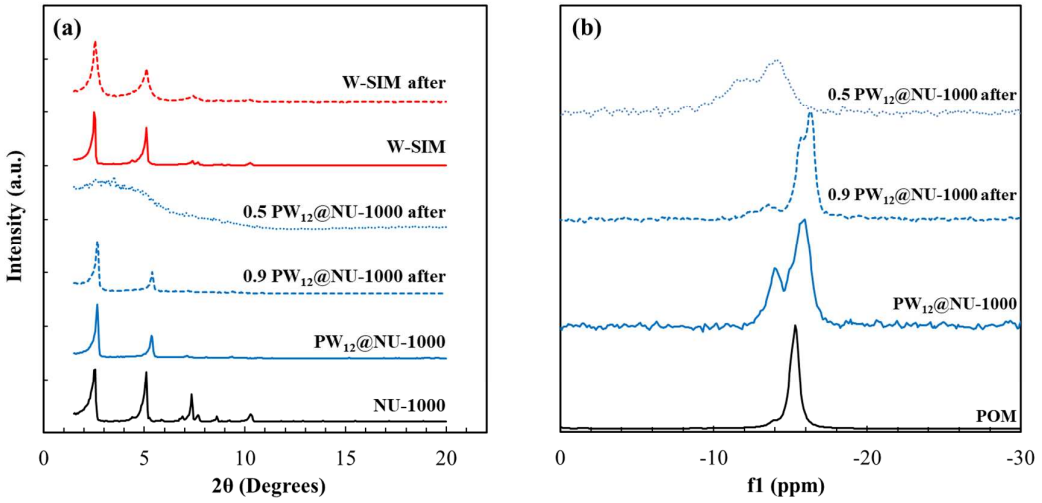

Figure 3. Bulk structure characterizations of catalysts (a) PXRD patterns, and (b) Solid-state ^{31}P CP MAS NMR

NMR and EXAFS help indicate the possible structures of the WO_x species present in these materials. Solid-state ^{31}P cross polarization magic angle spinning (CP MAS) NMR spectra (Figure 3b) confirm that the POM structure is intact upon synthesis and after the reaction. Pure (solid) POM presents a sharp peak at -15 ppm that is attributed to the symmetric central P atom,[51] and very small feature at -14 ppm. Kozhevnikov et. al. reported a feature at -14 ppm that increased with decreasing POM loading on silica.[52] In our case, this feature is intense in the as-synthesized catalyst and diminishes significantly after the reaction. Given that the material will dehydrate during reaction, we suggest that this feature is related to POM in a hydrated or hydroxyl-rich environment. We attribute the feature at -16 ppm in both fresh and used catalysts to the direct interaction of POM and the Zr_6 nodes of NU-1000.

EXAFS results support the presence of WO_x clusters in PW_{12}@NU-1000 and isolated W

atoms in W-SIM. Although the W coordination shells could not be readily fit in a quantitative manner, a strong feature centered around 3.2 Å in Figure 4a has been assigned to W-O-W scattering in WO_x clusters.[53] On the other hand, W-SIM does not present strong features in this regime, indicating negligible WO_x cluster formation (Table 1). Furthermore, the two peaks at 1.2 and 1.5 Å in Figure 4b are assigned to W=O and W–O, respectively. The stronger relative intensity of W=O to W–O in W-SIM compared to 0.9 PW_{12}@NU-1000 is further consistent with isolated WO_x sites in W-SIM and extended WO_x domains in 0.9 PW_{12}@NU-1000.

The low surface density and the EXAFS are both indicative of isolated WO_x groups in W-SIM, which in turn predicts that W-SIM would have negligible reactivity toward *o*-xylene isomerization. Isolated metal oxides cannot readily delocalize charge,[8] resulting in weak or absent Brønsted acid behavior.

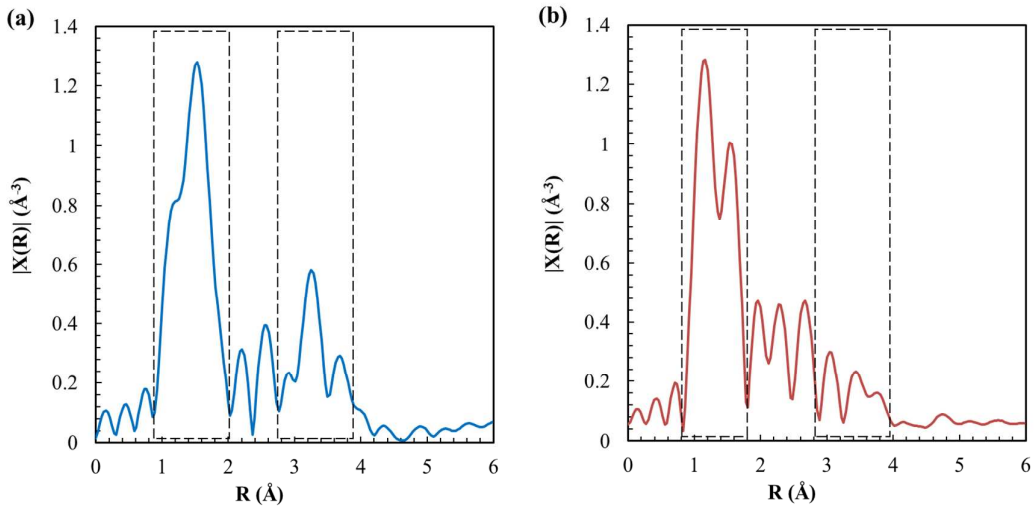

Figure 4. R-space EXAFS spectra of (a) 0.9 PW_{12}@NU-1000, and (b) W-SIM

Catalysis.

Previous reports state that *o*-xylene catalysis rates and selectivities are strongly dependent on the local WO_x structure.[8-9] Rates per W atom increase up to monolayer capacity for WO_x-ZrO_2 and then fall at higher loadings as WO_x becomes sterically inaccessible. Similarly, it has been reported that moderate POM loadings on TiO_2 surfaces are more favorable than either well-dispersed POMs or large aggregates of POMs. In the former, strong interactions with the

support limit the acidity, while in the latter, extended clusters of POMs limit acid site accessibility.[54]

Table 2. Summary of catalysis.[a]

Catalyst	Initial TOF [mol mol_W^{-1} hr^{-1}] [b]	Selectivity [%][c]	
		Isomerization	Disproportionation
WO_x-ZrO_2	0.11	100	0
NU-1000	< 0.01[d]	-	-
W-SIM	< 0.01[d]	-	-
0.5 PW_{12}@NU-1000[e]	< 0.01[d]	-	-
0.9 PW_{12}@NU-1000	0.16	17	83

[a] 50-100 mg catalyst (to match amount of W) to reach <10% conversion, 523 K in 10 sccm *o*-xylene/Ar and 10 sccm H_2 at nominal 1 bar pressure. Turnover frequencies are reproducible to ± 0.01 hr^{-1} and selectivities are reproducible to ± 2% across triplicate runs of three different catalyst synthesis batches. See experimental methods for full details.

[b] Extrapolated to 0 min from the trend of *o*-xylene conversion between 80 and 240 min.

[c] Isomerization (*m*- and *p*-xylene) or disproportionation (toluene and trimethylbenzene) products divided by total products at 240 min time-on-stream (TOS).

[d] TOF of 0.01 hr^{-1} reflects the detection limit of FID under the chosen conditions.

[e] Catalysts 0.3, 0.4, and 0.7 PW_{12}@NU-1000 catalysts are similarly unreactive.

Table 2 compares reactivities and selectivities of the four catalysts at 523 K. This temperature was chosen because product yields were below detectable limits for all NU-1000 based catalysts at lower temperatures (423 and 473 K). Future work will address whether this represents a critical temperature to activate the material or a high apparent activation energy. At one extreme, W-SIM is inactive for *o*-xylene catalysis at 523 K, as predicted by its site isolation. At the other extreme, WO_x-ZrO_2 is active and stable with time-on-stream (Figure S4), consistent with its well-established use in this reaction. Like W-SIM, 0.5 PW_{12}@NU-1000 also showed no activity at any time, but in this case, this result conflicts with the expected strong acidity of the POM unit, indicating that the POM and/or MOF structure collapsed during the catalyst pre-heating to 523 K or immediately upon the start of the reaction. In contrast, 0.9 PW_{12}@NU-1000 shows initial reactivity (per W atom basis) even higher than WO_x-ZrO_2. To understand the difference between these two catalysts, we note that with the absence of activity, 0.5 PW_{12}@NU-1000 lost most of its surface area (70 m^2/g) and porosity (Figure 2). Likewise, the long-range NU-1000 crystal structure of 0.5 PW_{12}@NU-1000 collapsed, (Figure 3a) and this occurred even prior to catalysis, during the catalyst pre-heating (Figure S5). Lastly, 0.5 PW_{12}@NU-1000 also lost integrity of the POM

cluster, as shown by the loss of the features at -15 and -16 ppm, and their replacement by broad features between -10 and -14 ppm (Figure 3b). Instability of POM in harsh catalytic conditions as well as deactivation has been reported for many other POM systems.[55-56] Although not listed in Table 2, similarly-synthesized catalysts with POM loadings from 0.3 to 0.7 POM per Zr_6 node also showed no activity at any time, and for none of these was the long-range order maintained after the catalytic test (Figure S6). In contrast, the crystal structure of the bare NU-1000 support was retained after catalytic conditions (Figure S7), and likewise, the pore dimensions (Figure 2b), long-range crystal (Figure 3a) and POM structure (Figure 3b) of the catalytically active 0.9 PW_{12}@NU-1000. Maximal loading of POM within the NU-1000 framework appears to synergistically stabilize both the POM and the MOF structure.

The absence of reactivity for low loadings may have analogies to other studies in which, for example, catalysts of low POM loadings on silica support show less activity for alkane isomerization. In such cases, isolated POM clusters coordinate with three surface silanols, leaving no available protons for acid catalysis.[57-58] In contrast, completely filling the MOF with POMs appears to physically prop open the catalyst structure in much the same way that one would pillar a clay material,[59-61] preventing loss of long-range order and catalytic reactivity. PTA is known to have a particularly strong interaction with ZrO_2,[62] which may cause the MOF to collapse around the POM if physically able. Although the POM clusters appear to be uniformly distributed within the NU-1000 (Figure S1), we cannot discount the idea that the POM cluster occupy differently-reactive sites in the NU-1000 at low and high loadings. Unfortunately, the complete collapse of the pore structure and reactivity at low POM loadings makes challenging a further understanding of the potential structural heterogeneity of the as-synthesized catalysts.

Although having good initial reactivity, 0.9 PW_{12}@NU-1000 deactivates gradually over time at 523 K, as shown in Figure 5a. Some activity is regained upon moving to a higher temperature, but the catalyst resumes deactivating immediately. This is similar behavior to many other microporous solid acid catalysts for C-C isomerization,[63,64,65] and it is generally ascribed to carbon deposition or strong adsorption of reaction intermediates on active sites. Further study and optimization of reaction conditions may be able to minimize its impact. As already noted, Figure 3a shows that this deactivation is not due to wholesale loss of the MOF long-range order, and Figure 3b confirms that the POMs remain intact, although there may be

some reorganization of POMs within the pores of the support. Also, Figure 2a and 2b indicate that meso- and micropores of NU-1000 are still present, and that the mesopores in particular have not changed in dimensions. Mass balance for this reaction is good (higher than 95%), excluding excessive coking, and there is no change to the physical appearance of the catalysts after the reactions.

While the organic ligands of the MOF prevent regenerating the catalyst by calcination, as well as precluding analysis of coke by TGA, no species were detected upon purge under inert flow at 573 K. This observation rules out the possibility of deactivation due to simple condensation of species within the pores.

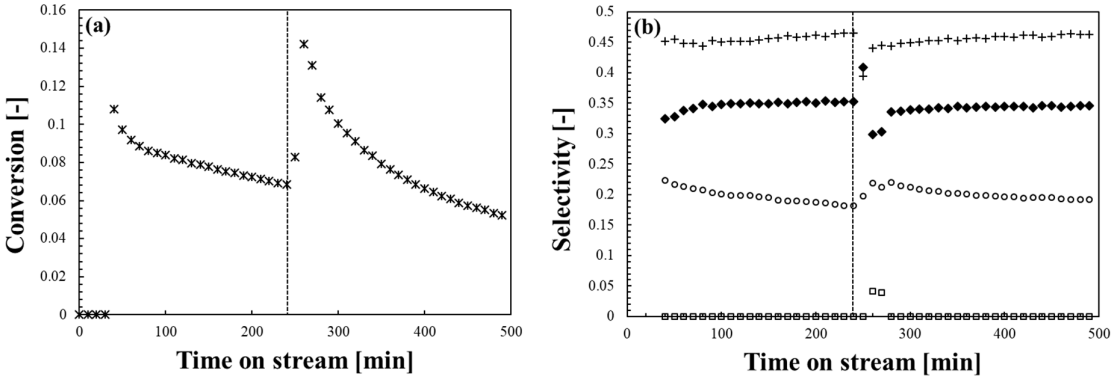

Figure 5. Representative time-on-stream: (a) conversion of *o*-xylene and (b) selectivities of products (♦: toluene, □: *p*-xylene, ○: *m*-xylene, +: 1,2,4-trimethylbenzene) over 0.9 PW_{12}@NU-1000 at 523 K (before 240 min) and 573 K (after 240 min).

Solid-state ^{13}C CP MAS NMR spectrum (Figure 6) of the used catalyst after inert purge 573 K shows a resonance at 17.8 ppm consistent with a mobile Ar-$\underline{C}H_3$ remaining within the catalyst. This species was successfully extracted with CD_2Cl_2, identified, and quantified by solution ^1H NMR as approximately 2 *o*-xylene molecules per POM cluster (Figure S8). Thus, the decrease in rates may be due to a slow approach to a steady state when the POMs become saturated with strongly bound reactants. Rate laws will be fully developed in future investigations over these materials.

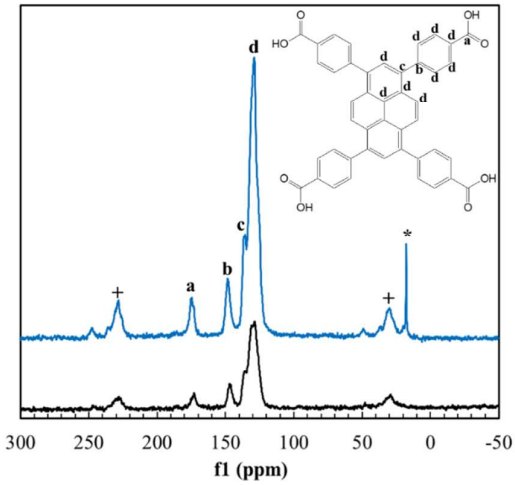

Figure 6. Solid-state ^{13}C CP MAS NMR spectra of 0.9 PW_{12}@NU-1000 as synthesized (black) and after catalysis (blue). + indicates spinning sidebands, * indicates new feature assigned as adsorbed $(C_6H_4)(\underline{C}H_3)_2$.

In addition to differences in rates, the catalysts promote different reaction pathways. Scheme 1 shows two representative *o*-xylene reaction pathways that different materials can promote. In the intramolecular isomerization pathway,[2] *o*-xylene is protonated at a Brønsted acid site. Then, a methyl group can shift from *ortho* to *meta* and further to *para*. At the low conversions used in these experiments, the selectivity to *p*-xylene is expected to be low, since two methyl shifts would be required before desorption from the active site. The experimental absence of *p*-xylene in these experiments also rules out direct *ortho* to *para* transitions that have been proposed for an intermolecular pathway[66] or from an extremely active catalyst.[67] In the intermolecular mechanism, two reactant molecules disproportionate to yield toluene and trimethylbenzene. The experiments strongly favor 1,2,4-trimethylbenzene over formation of 1,2,3-trimethylbenzene, as consistent with previous studies.[3, 68] Given the low conversion, the essentially zero yield of 1,3,5-trimethylbenzene is also expected. The disproportionation reaction is favored in materials with two adjacent active sites to accommodate migration of the proton from one ring to another. This mechanism has been reported to occur primarily in highly porous materials such as zeolites with relatively large channels (FAU, MOR, ZSM-12), where the xylene species are present in high local concentration.[1-2] Min et al. experimentally verified the formation of the diphenylmethane-based intermediate in zeolites that have large cavities or channels, and showed up to 99% disproportionation selectivity in such materials.[69]

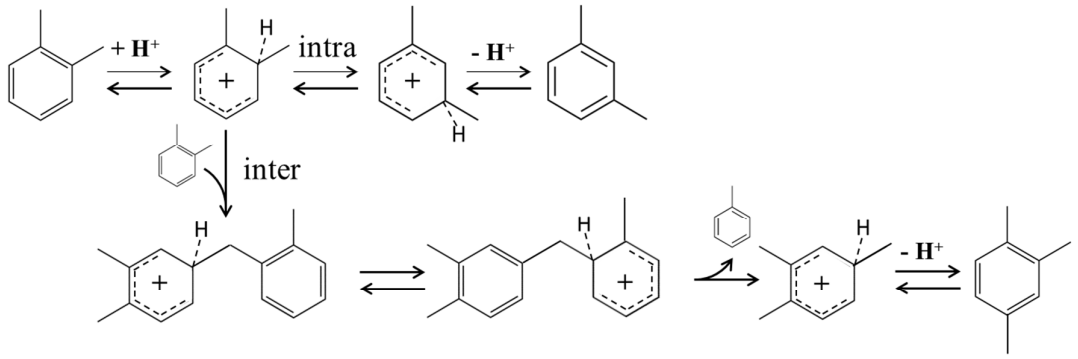

Scheme 1. *o*-xylene reaction pathways: intramolecular isomerization and intermolecular disproportionation

The WO_x-ZrO_2 reference exhibits the typical behavior for this catalyst,[9] with 100 % selectivity toward the isomerization pathway in differential conversion regime. In contrast, the product selectivity over 0.9 PW_{12}@NU1000 shows primarily *o*-xylene disproportionation, where 83% of the product consists of a near equimolar mixture of toluene and trimethylbenzene, with the remaining minority product being *m*-xylene. The high selectivity to the disproportionation products and the apparent strong chemisorption of *o*-xylene leads to the proposed catalyst structure of Figure 7. In this hypothesized structure for the working state of the catalyst, the POM is electrostatically bound to the node[52, 70-71] via one of the three H^+ of the POM. Recently, our team demonstrated via a crystallographic method that the HPA and the Zr_6 node are close enough[72] to be able to form a hydrogen bond, which we denote in Figure 7. We also note that at reaction temperatures, we would expect some mobility and disorder of the POM location within the support framework, leading to deviations from the crystallographically-determined structure. The remaining two H^+ lead to two chemisorbed *o*-xylene per POM, as seen in the extracted solution after catalysis (Figure S8). The chemisorption of *o*-xylene may be unusually strong because of the additional stabilizing influence of the MOF aromatic ligands, especially given the PXRD pattern evidence that the POM is likely found within the small triangular channels. We hypothesize that the location of the POM within the MOF structure provides unique environments for the two reaction pathways. The space between the POM and an adjacent linker (in the ab plane) only provides room for a single *o*-xylene (marked in orange in Figure 7), which could promote the isomerization pathway. In contrast, the triangular channels (above and below POMs along the c-axis) and the lateral cavities (between the two adjacent Zr_6 nodes along the c-axis) appear to be appropriately sized for the intermediate of the disproportionation pathway

(trimethylated diphenylmethane, marked with purple in Figure 7). These triangular channels are 1.2 nm, comparable to those of a large-pore acid zeolite, in which disproportionation is known to occur.[69]

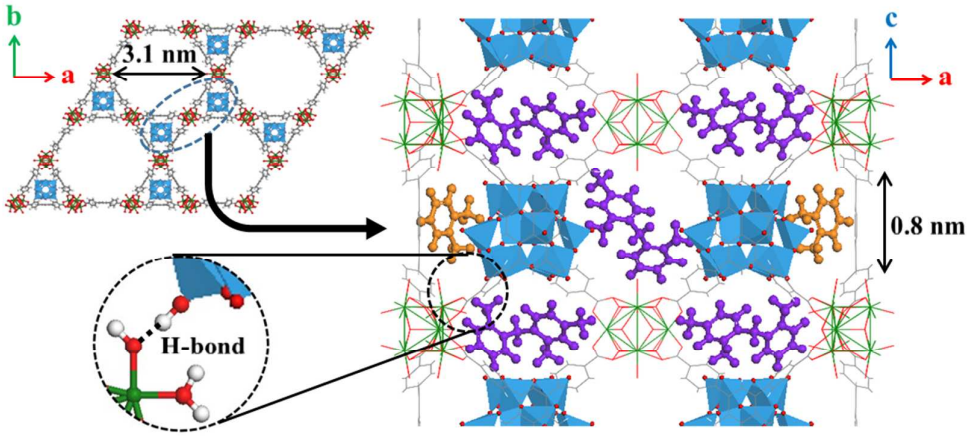

Figure 7. Proposed structure of PW_{12}@NU-1000. Color coded for potential reaction sites for isomerization (orange) and disproportionation (purple) under reaction conditions (right) and proposed hydrogen bond interaction under ambient condition (left bottom dotted circle). Dark green=Zr, Blue prisms=WO_5, red=O, gray=C, white=H

■ CONCLUSIONS

The Keggin POM of phosphotungstic acid was encapsulated in NU-1000 (PW_{12}@NU-1000), and this catalyst was shown to be active for the benchmark strong acid-catalyzed reaction of *o*-xylene isomerization/disproportionation at 523K. While MOFs display stable activities for many reactions, researchers have predominantly used MOFs as precursor, i.e. with deliberate decomposition of the framework,[37, 73-75] for use under aggressive conditions. This work demonstrates that MOF-supported catalysts can be structurally stable during C-C skeletal rearrangement reactions that have been widely used in industrial and academic investigations of porous solid acids, but never previously in MOFs. Indeed, maximal loading of ~1 Keggin unit per unit cell of NU-1000 appears to stabilize structures of both the PTA and NU-1000; lower loadings of PTA immediately lost all structural integrity under reaction conditions. Furthermore, WO_x installed by other methods, such as impregnation of tungsten amido complexes, gives isolated WO_x sites that are unreactive for this reaction. Finally, the structurally-stable PW_{12}@NU-1000 catalyst shows strongly atypical selectivity toward

disproportionation, which likely results from the particular pore structure of MOF support in which two Keggin units are stabilized in close proximity in the smaller (but still large relative to an aluminosilicate zeolite) side channels of the MOF. In the future, we expect that the tunable pore structure of MOFs via synthesis with different linkers will lead to new opportunities for controlling reaction pathway selectivity by placing the PTA in different pore environments or at different local densities. This control might enable a level of reaction network tuning which is not readily accessible with conventional oxide materials.

■ EXPERIMENTAL METHODS

Synthesis of Catalysts. The catalyst support, NU-1000, was synthesized and activated following the published literature.[76] The control material WO_x-ZrO_2 was synthesized via incipient wetness impregnation and calcined according to a protocol in the literature.[8] Phosphotungstic acid ($H_3PW_{12}O_{40}$) was encapsulated in NU-1000 (PW_{12}@NU-1000) via addition of PTA (2 eq. PTA to Zr_6 node for 0.9 PW_{12}@NU-1000 and 0.5 eq. PTA to Zr_6 node for 0.5 PW_{12}@NU-1000) dissolved in water following a procedure previously developed by our team.[48] For the synthesis of W-SIM (Solution phase grafting in MOFs), 200 mg of NU-1000 (92.6 μmol of Zr_6 node) and 235.1 μL (8 tungsten equivalents to one Zr_6 node) of bis(tert-butylimido)bis(dimethylamino)tungsten (VI) (Strem, min. 97% BTBMW) were dissolved in 5 mL heptane (99 %, anhydrous, Sigma Aldrich) in an argon-filled glove box for 24 h with occasional swirling. The mixture was decanted, and then mixed 5 mL of fresh heptane for 4 times to remove unreacted tungsten precursor. After this washing step, the material was transferred out from the glove box, and then a similar washing step was repeated but with acetone. Upon exposure to moist air, both amines and imines ligands from the tungsten precursor were removed to form tungsten oxide clusters on the nodes of NU-1000.[77]

Characterization of Catalysts. Tungsten (209.475, 209.860, 224.875, and 239.709 nm) and zirconium (327.305, 339.198, 343.832, and 349.621 nm) loadings were collected using inductively coupled plasma atomic emission spectroscopy (ICP-AES, iCAP 7600, Thermo Scientific). One mg amounts of catalysts were digested in 0.75 mL sulfuric acid (ACS reagent, 95-98 %, Sigma Aldrich) and 0.25 mL of 30 wt.% hydrogen peroxide (aqueous, Sigma Aldrich) solution with the aid of microwave using Initiator+ (Biotage) at 150 °C for 5

min.

Nitrogen physisorption isotherms at 77 K were collected using a Tristar II (Micromeritics), and DFT (Density Functional Theory) pore size distributions were derived from the desorption isotherms. Prior to the measurement, samples were dried at 120 °C under dynamic vacuum for 18 h using a Smart VacPrep (Micromeritics).

Powder X-ray diffraction (PXRD) patterns were collected on a SmartLab diffractometer (Rigaku) with a Cu-Kα radiation source (45 kV and 160 mA for tube voltage and current, respectively). Diffraction patterns were recorded over the 2θ range of 2–20° with a 0.05° step width and a 5°/min scan speed.

Solid-state CP MAS ^{13}C and ^{31}P NMR spectra were collected on a 400 MHz VNMRS spectrometer (Varian) equipped with a conventional triple resonance 5 mm probe-head in double resonance mode. Samples were packed in a zirconia rotor, and the spinning frequency was set at 10 kHz. Chemical shifts (δ [ppm]) were referenced to adamantane and $(NH_4)H_2PO_4$ for ^{13}C and ^{31}P, respectively. Solution ^{1}H NMR spectra were recorded on an AVANCE III 600 MHz (Bruker). Used catalysts were washed with CD_2Cl_2 (Cambridge Isotope Laboratories, D 99.8 %) to extract organic molecules from the samples. Spectra were obtained applying a 30° pulse, an acquisition time of 2.7s, a delay time of 5 s (after finding that the much longer delay value of 20 s did not affect the area ratios between STD and analyte), and accumulating 16 scans. Spectra were carefully phased and baseline corrected. Quantification was performed comparing the areas of the peaks of the reference compound (1,4-dimethoxybenzene) and the target compound (*o*-xylene). Spectra were collected at the IMSERC (Integrated Molecular Structure Education and Research Center) facility at Northwestern University.

W L_3-edge X-ray absorption spectroscopy (XAS) was performed at sector 5 of the Advanced Photon Source, Argonne National Laboratory, on the Dupont-Northwestern-Dow Collaborative Access Team (DND-CAT) bending magnet D beamline using a Si(111) double crystal monochromator. All measurements were performed in transmission mode with Canberra ionization chambers. Energies were calibrated against a W foil reference spectrum collected with each sample spectrum by setting the W foil first inflection point at the known W L_3-edge to 10207 eV. Catalysts pellets were pressed into specially made Al sample holders, dried under vacuum at 120 °C, then cooled and switched to flowing He before data collection.

Scans were performed with a 0.6 eV increment in the pre-edge region and 0.05 $Å^{-1}$ intervals between 3.0 $Å^{-1}$ < k < 14.0 $Å^{-1}$. Counting time per data point was increased from 1 to 5 s from beginning to end of scans to maximize signal count at high k. XAS spectra were processed in Athena using standard methods. Spectra were normalized by fitting a cubic polynomial to 150-700 eV above the edge and subtracting the expected absorption at the edge. The background was removed using the AUTOBK algorithm with R=1.0 and spline range from 0.5 $Å^{-1}$ < k < 13.5 $Å^{-1}$ when computing $\chi(k)$. The Fourier transform was performed on the k^2-weighted $\chi(k)$ function over the range 3 $Å^{-1}$ < k < 12.8 $Å^{-1}$ using a Hanning window function with width dk = 0.5 $Å^{-1}$.

Catalysis. Kinetic studies were carried out in a flow reactor at 523 K using 50-100 mg of catalysts to maintain differential conversion regime (< 10%). Catalysts that were supported on quartz wool were loaded in a quartz tube reactor. The reactor was heated to 523 K with a ramp rate of 5.0 K/min under flow of H_2 (10 mL/min, 99.999%, Airgas). *o*-xylene (≥ 99.0%, Sigma-Aldrich) was introduced by Ar (10 mL/min, 99.999%, Airgas) bubbler with a total pressure of 1 bar at 298 K (0.87 kPa of reactant). Reactions were carried out at 523 K for 4 h, and then heated at 5.0 K/min to 573 K for 4 hours under same flow condition. Subsequently, only Ar (20 mL/min) was supplied throughout the system to remove physisorbed species for 6 h at 573 K. Gas flow rates were controlled by mass flow controllers (Altamira Instruments). Online products identification and quantification were performed by a 7890 A GC (Agilent Technologies) equipped with a flame ionization detector (FID) and HP-INNOWAX (30 m length, 0.32 mm diameter, 0.15 mm film). The mass balance with respect to the products and unreacted *o*-xylene for all runs exceeded 95%. Initial turnover frequencies were calculated based on conversions extrapolated linearly to time at 0 min from the trend of time-on-stream *o*-xylene conversion between 80 and 240 min. The reaction and online GC analysis were performed in Clean Cat core facility at Northwestern University.

■ ASSOCIATED CONTENT

Supporting Information

The Supporting Information is available free of charge on the ACS Publications website at DOI: XXX. Additional characterization data and kinetic data (PDF)

■ AUTHOR INFORMATION

Corresponding Author

* Email: o-farha@northwestern.edu, j-notestein@northwestern.edu

Author Contributions

The manuscript was written through contributions of all authors. All authors have given approval to the final version of the manuscript.

Notes

The authors declare no competing financial interest.

■ ACKNOWLEDGMENTS

Authors gratefully acknowledge the financial support from the Inorganometallic Catalyst Design Center, an EFRC funded by the DOE, Office of Basic Energy Sciences (DE-SC0012702). S.L.N. acknowledges the financial support from the National Science Foundation Graduate Research Fellowship under Grant No. DGE-1324585. Metal analysis was performed at the Northwestern University Quantitative Bio-element Imaging Center. This work made use of the J.B. Cohen X-ray Diffraction Facility supported by the MRSEC program of the National Science Foundation (DMR-1720139) at the Materials Research Center of Northwestern University and the Soft and Hybrid Nanotechnology Experimental (SHyNE) Resource (NSF ECCS-1542205, NSF DMR-0521267). This work also made use of the IMSERC at Northwestern University, which has received support from the Soft and

Hybrid Nanotechnology Experimental (SHyNE) Resource (NSF ECCS-1542205); the State of Illinois and International Institute for Nanotechnology (IIN). The CleanCat Core facility acknowledges funding from the Department of Energy (DE-SC0001329) used for the purchase of the Altamira BenchCat 4000. This research used resources of the Advanced Photon Source, a U.S. Department of Energy (DOE) Office of Science User Facility operated for the DOE Office of Science by Argonne National Laboratory under Contract No. DE-AC02-06CH11357.

■ REFERENCES

(1) Martens, J. A.; Perez-Pariente, J.; Sastre, E.; Corma, A.; Jacobs, P. A., Isomerization and disproportionation of m-xylene: Selectivities Induced by the Void Structure of the Zeolite Framework. *Appl. Catal.* **1988,** *45*, 85-101.
(2) Guisnet, M.; Gnep, N. S.; Morin, S., Mechanisms of xylene isomerization over acidic solid catalysts. *Micropor. Mesopor. Mat.* **2000,** *35-36*, 47-59.
(3) Lanewala, M. A.; Bolton, A. P., Isomerization of the xylenes using zeolite catalysts. *J. Org. Chem.* **1969,** *34*, 3107-3112.
(4) Hino, M.; Arata, K., Synthesis of solid superacid of tungsten oxide supported on zirconia and its catalytic action for reactions of butane and pentane. *J. Chem. Soc., Chem. Commun.* **1988**, 1259-1260.
(5) Soultanidis, N.; Zhou, W.; Psarras, A. C.; Gonzalez, A. J.; Iliopoulou, E. F.; Kiely, C. J.; Wachs, I. E.; Wong, M. S., Relating n-Pentane Isomerization Activity to the Tungsten Surface Density of WOx/ZrO2. *J. Am. Chem. Soc.* **2010,** *132*, 13462-13471.
(6) Larsen, G.; Lotero, E.; Petkovic, L. a. M.; Shobe, D. S., Alcohol Dehydration Reactions over Tungstated Zirconia Catalysts. *J. Catal.* **1997,** *169*, 67-75.
(7) Rorrer, J.; He, Y.; Toste, F. D.; Bell, A. T., Mechanism and kinetics of 1-dodecanol etherification over tungstated zirconia. *J. Catal.* **2017,** *354*, 13-23.
(8) Barton, D. G.; Shtein, M.; Wilson, R. D.; Soled, S. L.; Iglesia, E., Structure and Electronic Properties of Solid Acids Based on Tungsten Oxide Nanostructures. *J. Phys. Chem. B* **1999,** *103*, 630-640.
(9) Wilson, R. D.; Barton, D. G.; Baertsch, C. D.; Iglesia, E., Reaction and Deactivation Pathways in Xylene Isomerization on Zirconia Modified by Tungsten Oxide. *J. Catal.* **2000,** *194*, 175-187.
(10) Baertsch, C. D.; Soled, S. L.; Iglesia, E., Isotopic and Chemical Titration of Acid Sites in Tungsten Oxide Domains Supported on Zirconia. *J. Phys. Chem. B* **2001,** *105*, 1320-1330.
(11) Barton, D. G.; Soled, S. L.; Iglesia, E., Solid acid catalysts based on supported tungsten oxides. *Top. Catal.* **1998,** *6*, 87-99.
(12) Wang, Y.; Hou, Y.; Song, H., Ring-closing depolymerization of polytetrahydrofuran to produce tetrahydrofuran using heteropolyacid as catalyst. *Polym. Degrad. Stab.* **2017,** *144*, 17-23.
(13) Nie, G.; Li, G.; Liang, D.; Zhang, X., Alkylation of toluene with cyclohexene over phosphotungstic acid: A combined experimental and computational study. *J. Catal.* **2017,** *355*, 145-155.
(14) Kukovecz, Á.; Balogi, Z.; Kónya, Z.; Toba, M.; Lentz, P.; Niwa, S. I.; Mizukami, F.; Molnár, Á.; Nagy, J. B.; Kiricsi, I., Synthesis, characterisation and catalytic applications of sol–gel derived silica–phosphotungstic acid composites. *Appl. Catal., A.* **2002,** *228*, 83-94.
(15) Devassy, B. M.; Shanbhag, G. V.; Lefebvre, F.; Böhringer, W.; Fletcher, J.; Halligudi, S. B., Zirconia-supported phosphotungstic acid as catalyst for alkylation of phenol with benzyl alcohol. *J. Mol. Catal. A: Chem.* **2005,** *230*, 113-119.
(16) Macht, J.; Janik, M. J.; Neurock, M.; Iglesia, E., Mechanistic Consequences of Composition in Acid Catalysis by Polyoxometalate Keggin Clusters. *J. Am. Chem. Soc.* **2008,** *130*, 10369-10379.
(17) Ma, L.; Abney, C.; Lin, W., Enantioselective catalysis with homochiral metal-organic frameworks. *Chem. Soc. Rev.* **2009,** *38*, 1248-1256.
(18) Lee, J.; Farha, O. K.; Roberts, J.; Scheidt, K. A.; Nguyen, S. T.; Hupp, J. T., Metal-organic framework materials as catalysts. *Chem. Soc. Rev.* **2009,** *38*, 1450-1459.
(19) Hendon, C. H.; Rieth, A. J.; Korzyński, M. D.; Dincă, M., Grand Challenges and Future

Opportunities for Metal–Organic Frameworks. *ACS Cent. Sci.* **2017,** *3*, 554-563.
(20) Rimoldi, M.; Howarth, A. J.; DeStefano, M. R.; Lin, L.; Goswami, S.; Li, P.; Hupp, J. T.; Farha, O. K., Catalytic Zirconium/Hafnium-Based Metal–Organic Frameworks. *ACS Catal.* **2017,** *7*, 997-1014.
(21) Li, Z.; Schweitzer, N. M.; League, A. B.; Bernales, V.; Peters, A. W.; Getsoian, A. B.; Wang, T. C.; Miller, J. T.; Vjunov, A.; Fulton, J. L.; Lercher, J. A.; Cramer, C. J.; Gagliardi, L.; Hupp, J. T.; Farha, O. K., Sintering-Resistant Single-Site Nickel Catalyst Supported by Metal–Organic Framework. *J. Am. Chem. Soc.* **2016,** *138*, 1977-1982.
(22) Ahn, S.; Thornburg, N. E.; Li, Z.; Wang, T. C.; Gallington, L. C.; Chapman, K. W.; Notestein, J. M.; Hupp, J. T.; Farha, O. K., Stable Metal–Organic Framework-Supported Niobium Catalysts. *Inorg. Chem.* **2016,** *55*, 11954-11961.
(23) Murray, L. J.; Dinca, M.; Long, J. R., Hydrogen storage in metal-organic frameworks. *Chem. Soc. Rev.* **2009,** *38*, 1294-1314.
(24) Farha, O. K.; Özgür Yazaydın, A.; Eryazici, I.; Malliakas, C. D.; Hauser, B. G.; Kanatzidis, M. G.; Nguyen, S. T.; Snurr, R. Q.; Hupp, J. T., De novo synthesis of a metal–organic framework material featuring ultrahigh surface area and gas storage capacities. *Nat. Chem.* **2010,** *2*, 944-948.
(25) Furukawa, H.; Ko, N.; Go, Y. B.; Aratani, N.; Choi, S. B.; Choi, E.; Yazaydin, A. Ö.; Snurr, R. Q.; O′Keeffe, M.; Kim, J.; Yaghi, O. M., Ultrahigh Porosity in Metal-Organic Frameworks. *Science* **2010,** *329*, 424-428.
(26) Grunker, R.; Bon, V.; Muller, P.; Stoeck, U.; Krause, S.; Mueller, U.; Senkovska, I.; Kaskel, S., A new metal-organic framework with ultra-high surface area. *Chem. Commun.* **2014,** *50*, 3450-3452.
(27) McDonald, T. M.; Mason, J. A.; Kong, X.; Bloch, E. D.; Gygi, D.; Dani, A.; Crocella, V.; Giordanino, F.; Odoh, S. O.; Drisdell, W. S.; Vlaisavljevich, B.; Dzubak, A. L.; Poloni, R.; Schnell, S. K.; Planas, N.; Lee, K.; Pascal, T.; Wan, L. F.; Prendergast, D.; Neaton, J. B.; Smit, B.; Kortright, J. B.; Gagliardi, L.; Bordiga, S.; Reimer, J. A.; Long, J. R., Cooperative insertion of CO2 in diamine-appended metal-organic frameworks. *Nature* **2015,** *519*, 303-308.
(28) Teplensky, M. H.; Fantham, M.; Li, P.; Wang, T. C.; Mehta, J. P.; Young, L. J.; Moghadam, P. Z.; Hupp, J. T.; Farha, O. K.; Kaminski, C. F.; Fairen-Jimenez, D., Temperature Treatment of Highly Porous Zirconium-Containing Metal–Organic Frameworks Extends Drug Delivery Release. *J. Am. Chem. Soc.* **2017,** *139*, 7522-7532.
(29) Kreno, L. E.; Leong, K.; Farha, O. K.; Allendorf, M.; Van Duyne, R. P.; Hupp, J. T., Metal–Organic Framework Materials as Chemical Sensors. *Chem. Rev.* **2012,** *112*, 1105-1125.
(30) Stassen, I.; Burtch, N.; Talin, A.; Falcaro, P.; Allendorf, M.; Ameloot, R., An updated roadmap for the integration of metal-organic frameworks with electronic devices and chemical sensors. *Chem. Soc. Rev.* **2017,** *46*, 3185-3241.
(31) Mondloch, J. E.; Katz, M. J.; Planas, N.; Semrouni, D.; Gagliardi, L.; Hupp, J. T.; Farha, O. K., Are Zr6-based MOFs water stable? Linker hydrolysis vs. capillary-force-driven channel collapse. *Chem. Commun.* **2014,** *50*, 8944-8946.
(32) Howarth, A. J.; Liu, Y.; Li, P.; Li, Z.; Wang, T. C.; Hupp, J. T.; Farha, O. K., Chemical, thermal and mechanical stabilities of metal–organic frameworks. *Nat. Rev. Mater.* **2016,** *1*, 15018.
(33) Li, Z.; Peters, A. W.; Platero-Prats, A. E.; Liu, J.; Kung, C.-W.; Noh, H.; DeStefano, M. R.; Schweitzer, N. M.; Chapman, K. W.; Hupp, J. T.; Farha, O. K., Fine-Tuning the Activity of Metal–Organic Framework-Supported Cobalt Catalysts for the Oxidative Dehydrogenation of Propane. *J. Am. Chem. Soc.* **2017,** *139*, 15251-15258.
(34) Kim, I. S.; Li, Z.; Zheng, J.; Platero-Prats, A. E.; Mavrandonakis, A.; Pellizzeri, S.; Ferrandon, M.; Vjunov, A.; Gallington, L. C.; Webber, T. E.; Vermeulen, N. A.; Penn, R. L.;

Getman, R. B.; Cramer, C. J.; Chapman, K. W.; Camaioni, D. M.; Fulton, J. L.; Lercher, J. A.; Farha, O. K.; Hupp, J. T.; Martinson, A. B. F., Sinter-Resistant Platinum Catalyst Supported by Metal–Organic Framework. *Angew. Chem. Int. Ed.* **2018,** *57*, 909-913.
(35) Mondloch, J. E.; Bury, W.; Fairen-Jimenez, D.; Kwon, S.; DeMarco, E. J.; Weston, M. H.; Sarjeant, A. A.; Nguyen, S. T.; Stair, P. C.; Snurr, R. Q.; Farha, O. K.; Hupp, J. T., Vapor-Phase Metalation by Atomic Layer Deposition in a Metal–Organic Framework. *J. Am. Chem. Soc.* **2013,** *135*, 10294-10297.
(36) Zhang, Y.; Degirmenci, V.; Li, C.; Hensen, E. J. M., Phosphotungstic Acid Encapsulated in Metal–Organic Framework as Catalysts for Carbohydrate Dehydration to 5-Hydroxymethylfurfural. *ChemSusChem* **2011,** *4*, 59-64.
(37) Wang, P.; Feng, J.; Zhao, Y.; Wang, S.; Liu, J., MOF-Derived Tungstated Zirconia as Strong Solid Acids toward High Catalytic Performance for Acetalization. *ACS Appl. Mater. Interfaces* **2016,** *8*, 23755-23762.
(38) Vermoortele, F.; Ameloot, R.; Alaerts, L.; Matthessen, R.; Carlier, B.; Fernandez, E. V. R.; Gascon, J.; Kapteijn, F.; De Vos, D. E., Tuning the catalytic performance of metal-organic frameworks in fine chemistry by active site engineering. *J. Mater. Chem.* **2012,** *22*, 10313-10321.
(39) Zang, Y.; Shi, J.; Zhang, F.; Zhong, Y.; Zhu, W., Sulfonic acid-functionalized MIL-101 as a highly recyclable catalyst for esterification. *Catal. Sci. Technol.* **2013,** *3*, 2044-2049.
(40) Khder, A. E. R. S.; Hassan, H. M. A.; El-Shall, M. S., Metal-organic frameworks with high tungstophosphoric acid loading as heterogeneous acid catalysts. *Appl. Catal., A.* **2014,** *487*, 110-118.
(41) Wan, H.; Chen, C.; Wu, Z.; Que, Y.; Feng, Y.; Wang, W.; Wang, L.; Guan, G.; Liu, X., Encapsulation of Heteropolyanion-Based Ionic Liquid within the Metal–Organic Framework MIL-100(Fe) for Biodiesel Production. *ChemCatChem* **2015,** *7*, 441-449.
(42) Li, B.; Leng, K.; Zhang, Y.; Dynes, J. J.; Wang, J.; Hu, Y.; Ma, D.; Shi, Z.; Zhu, L.; Zhang, D.; Sun, Y.; Chrzanowski, M.; Ma, S., Metal–Organic Framework Based upon the Synergy of a Brønsted Acid Framework and Lewis Acid Centers as a Highly Efficient Heterogeneous Catalyst for Fixed-Bed Reactions. *J. Am. Chem. Soc.* **2015,** *137*, 4243-4248.
(43) Nguyen, L. T. L.; Nguyen, C. V.; Dang, G. H.; Le, K. K. A.; Phan, N. T. S., Towards applications of metal–organic frameworks in catalysis: Friedel–Crafts acylation reaction over IRMOF-8 as an efficient heterogeneous catalyst. *J. Mol. Catal. A: Chem.* **2011,** *349*, 28-35.
(44) Peters, A. W.; Li, Z.; Farha, O. K.; Hupp, J. T., Atomically Precise Growth of Catalytically Active Cobalt Sulfide on Flat Surfaces and within a Metal–Organic Framework via Atomic Layer Deposition. *ACS Nano* **2015,** *9*, 8484-8490.
(45) Noh, H.; Cui, Y.; Peters, A. W.; Pahls, D. R.; Ortuño, M. A.; Vermeulen, N. A.; Cramer, C. J.; Gagliardi, L.; Hupp, J. T.; Farha, O. K., An Exceptionally Stable Metal–Organic Framework Supported Molybdenum(VI) Oxide Catalyst for Cyclohexene Epoxidation. *J. Am. Chem. Soc.* **2016,** *138*, 14720-14726.
(46) Rimoldi, M.; Bernales, V.; Borycz, J.; Vjunov, A.; Gallington, L. C.; Platero-Prats, A. E.; Kim, I. S.; Fulton, J. L.; Martinson, A. B. F.; Lercher, J. A.; Chapman, K. W.; Cramer, C. J.; Gagliardi, L.; Hupp, J. T.; Farha, O. K., Atomic Layer Deposition in a Metal–Organic Framework: Synthesis, Characterization, and Performance of a Solid Acid. *Chem. Mater.* **2017,** *29*, 1058-1068.
(47) Cui, Y.; Rimoldi, M.; Platero-Prats, A. E.; Chapman, K. W.; Hupp, J. T.; Farha, O. K., Stabilizing a Vanadium Oxide Catalyst via Supporting on Metal-Organic Framework. *ChemCatChem* **2018,** *10*, 1772-1777.
(48) Buru, C. T.; Li, P.; Mehdi, B. L.; Dohnalkova, A.; Platero-Prats, A. E.; Browning, N. D.; Chapman, K. W.; Hupp, J. T.; Farha, O. K., Adsorption of a Catalytically Accessible

Polyoxometalate in a Mesoporous Channel-type Metal–Organic Framework. *Chem. Mater.* **2017,** *29*, 5174-5181.
(49) Nawrocki, J.; Rigney, M.; McCormick, A.; Carr, P. W., Chemistry of zirconia and its use in chromatography. *J. Chromatogr. A* **1993,** *657*, 229-282.
(50) Kouva, S.; Honkala, K.; Lefferts, L.; Kanervo, J., Review: monoclinic zirconia, its surface sites and their interaction with carbon monoxide. *Catal. Sci. Technol.* **2015,** *5*, 3473-3490.
(51) Sofia, L. T. A.; Krishnan, A.; Sankar, M.; Kala Raj, N. K.; Manikandan, P.; Rajamohanan, P. R.; Ajithkumar, T. G., Immobilization of Phosphotungstic Acid (PTA) on Imidazole Functionalized Silica: Evidence for the Nature of PTA Binding by Solid State NMR and Reaction Studies. *J. Phys. Chem. C* **2009,** *113*, 21114-21122.
(52) Kozhevnikov, I. V.; Kloetstra, K. R.; Sinnema, A.; Zandbergen, H. W.; van Bekkum, H., Study of catalysts comprising heteropoly acid H3PW12O40 supported on MCM-41 molecular sieve and amorphous silica. *J. Mol. Catal. A: Chem.* **1996,** *114*, 287-298.
(53) Kochubey, D. I.; Berdnikova, P. V.; Pai, Z. P.; Chesalov, Y. A.; Kanazhevskiy, V. V.; Khlebnikova, T. B., Structure and properties of tungsten peroxopolyoxo complexes – promising catalysts for organics oxidation. II: Cation type influence on the tungsten peroxocomplex structure. *J. Mol. Catal. A: Chem.* **2013,** *366*, 341-346.
(54) Ladera, R. M.; Ojeda, M.; Fierro, J. L. G.; Rojas, S., TiO2-supported heteropoly acid catalysts for dehydration of methanol to dimethyl ether: relevance of dispersion and support interaction. *Catal. Sci. Technol.* **2015,** *5*, 484-491.
(55) Kozhevnikov, I. V., Catalysis by Heteropoly Acids and Multicomponent Polyoxometalates in Liquid-Phase Reactions. *Chem. Rev.* **1998,** *98*, 171-198.
(56) Misono, M., Heterogeneous Catalysis by Heteropoly Compounds of Molybdenum and Tungsten. *Catal. Rev.* **1987,** *29*, 269-321.
(57) Bardin, B. B.; Davis, R. J., Effect of water on silica-supported phosphotungstic acid catalysts for 1-butene double bond shift and alkane skeletal isomerization. *Appl. Catal., A* **2000,** *200*, 219-231.
(58) Grinenval, E.; Garron, A.; Lefebvre, F.; #xe9; #xe9; ric, n-Butane Isomerization over Silica-Supported Heteropolyacids: Study of Some Parameters. *J. Catal.* **2013,** *2013*, 8.
(59) Figueras, F., Pillared Clays as Catalysts. *Catal. Rev.* **1988,** *30*, 457-499.
(60) Lee, W. Y.; Raythatha, R. H.; Tatarchuk, B. J., Pillared-clay catalysts containing mixed-metal complexes: I. Preparation and characterization. *J. Catal.* **1989,** *115*, 159-179.
(61) Lambert, J.-F.; Poncelet, G., Acidity in pillared clays: origin and catalytic manifestations. *Top. Catal.* **1997,** *4*, 43-56.
(62) Zhu, S.; Zhu, Y.; Hao, S.; Zheng, H.; Mo, T.; Li, Y., One-step hydrogenolysis of glycerol to biopropanols over Pt-H4SiW12O40/ZrO2 catalysts. *Green Chem.* **2012,** *14*, 2607-2616.
(63) van Donk, S.; Bitter, J. H.; de Jong, K. P., Deactivation of solid acid catalysts for butene skeletal isomerisation: on the beneficial and harmful effects of carbonaceous deposits. *Appl. Catal. A Gen.* **2001,** *212*, 97-116.
(64) Srivastava, R.; Choi, M.; Ryoo, R., Mesoporous materials with zeolite framework: remarkable effect of the hierarchical structure for retardation of catalyst deactivation. *Chem. Commun.* **2006**, 4489-4491.
(65) Wang, P.; Zhang, W.; Zhang, Q.; Xu, Z.; Yang, C.; Li, C., Comparative study of n-butane isomerization over SO42−/Al2O3-ZrO2 and HZSM-5 zeolites at low reaction temperatures. *Appl. Catal. A Gen.* **2018,** *550*, 98-104.
(66) Beck, J. S.; Haag, W. O.; Buonomo, F.; Sanfilippo, D.; Trifirò, F.; Arnold, H.; Döbert, F.; Gaube, J., Organic Reactions: Sections 4.1 – 4.4. *Wiley-VCH Verlag GmbH*: **2008** pp 2123-2231.

(67) Corma, A.; Iborra, S.; Mifsud, M.; Renz, M., A new, alternative, halogen-free synthesis for the fragrance compound Melonal using zeolites and mesoporous materials as oxidation catalysts. *Journal of Catalysis* **2005,** *234*, 96-100.
(68) Collins, D. J.; Mulrooney, K. J.; Medina, R. J.; Davis, B. H., Xylene isomerization and disproportionation over lanthanum Y catalyst. *J. Catal.* **1982,** *75*, 291-301.
(69) Min, H.-K.; Cha, S. H.; Hong, S. B., Mechanistic Insights into the Zeolite-Catalyzed Isomerization and Disproportionation of m-Xylene. *ACS Catal.* **2012,** *2*, 971-981.
(70) Su, F.; Wu, Q.; Song, D.; Zhang, X.; Wang, M.; Guo, Y., Pore morphology-controlled preparation of ZrO2-based hybrid catalysts functionalized by both organosilica moieties and Keggin-type heteropoly acid for the synthesis of levulinate esters. *J. Mater. Chem. A* **2013,** *1*, 13209-13221.
(71) Paille, G.; Gomez-Mingot, M.; Roch-Marchal, C.; Lassalle-Kaiser, B.; Mialane, P.; Fontecave, M.; Mellot-Draznieks, C.; Dolbecq, A., A Fully Noble Metal-Free Photosystem Based on Cobalt-Polyoxometalates Immobilized in a Porphyrinic Metal–Organic Framework for Water Oxidation. *J. Am. Chem. Soc.* **2018**.
(72) Buru, C. T.; Platero-Prats, A. E.; Chica, D. G.; Kanatzidis, M. G.; Chapman, K. W.; Farha, O. K., Thermally induced migration of a polyoxometalate within a metal-organic framework and its catalytic effects. *J. Mater. Chem. A* **2018,** *6*, 7389-7394.
(73) Malonzo, C. D.; Shaker, S. M.; Ren, L.; Prinslow, S. D.; Platero-Prats, A. E.; Gallington, L. C.; Borycz, J.; Thompson, A. B.; Wang, T. C.; Farha, O. K.; Hupp, J. T.; Lu, C. C.; Chapman, K. W.; Myers, J. C.; Penn, R. L.; Gagliardi, L.; Tsapatsis, M.; Stein, A., Thermal Stabilization of Metal–Organic Framework-Derived Single-Site Catalytic Clusters through Nanocasting. *J. Am. Chem. Soc.* **2016,** *138*, 2739-2748.
(74) Yan, X.; Lu, N.; Fan, B.; Bao, J.; Pan, D.; Wang, M.; Li, R., Synthesis of mesoporous and tetragonal zirconia with inherited morphology from metal-organic frameworks. *CrystEngComm* **2015,** *17*, 6426-6433.
(75) Tang, J.; Salunkhe, R. R.; Liu, J.; Torad, N. L.; Imura, M.; Furukawa, S.; Yamauchi, Y., Thermal Conversion of Core–Shell Metal–Organic Frameworks: A New Method for Selectively Functionalized Nanoporous Hybrid Carbon. *J. Am. Chem. Soc.* **2015,** *137*, 1572-1580.
(76) Wang, T. C.; Vermeulen, N. A.; Kim, I. S.; Martinson, A. B. F.; Stoddart, J. F.; Hupp, J. T.; Farha, O. K., Scalable synthesis and post-modification of a mesoporous metal-organic framework called NU-1000. *Nat. Protoc.* **2016,** *11*, 149-162.
(77) Liu, T.-F.; Vermeulen, N. A.; Howarth, A. J.; Li, P.; Sarjeant, A. A.; Hupp, J. T.; Farha, O. K., Adding to the Arsenal of Zirconium-Based Metal–Organic Frameworks: the Topology as a Platform for Solvent-Assisted Metal Incorporation. *Eur. J. Inorg. Chem.* **2016,** *2016*, 4349-4352.

TOC graphic